

Magnetic frustrations in the face centered cubic antiferromagnet NiS₂

M. Matsuura^{1,3}, Y. Endoh^{2,3}, H. Hiraka², K. Yamada⁴, K. Hirota¹, A. S. Mishchenko^{5,6}, N. Nagaosa^{5,7} and I. V. Solovyev^{8,9}

¹*Department of Physics, Tohoku University, Sendai 980-8578, Japan*

²*Institute for Materials Research, Tohoku University, Katahira, Aoba-ku, Sendai 980-8577, Japan*

³*Core Research for Evolutional Science and Technology, JST, Kawaguchi 332-0012, Japan*

⁴*Institute of Chemical Research, Gokasho, Uji, Kyoto 611-0011, Japan*

⁵*Correlated Electron Research Center, Tsukuba, Ibaraki 305-0046, Japan*

⁶*Russian Research Centre “Kurchatov Institute”, 123182 Moscow, Russia*

⁷*Department of Applied Physics, University of Tokyo, Bunkyo-ku, Tokyo 113-8656, Japan*

⁸*JRCAT-Angstrom Technology Partnership, Tsukuba, Ibaraki 305-0046, Japan*

⁹*Institute of Metal Physics, Russian Academy of Sciences, Ekaterinburg GSP-170, Russia*

(November 9, 2018)

Neutron scattering experiment on NiS₂ single crystal revealed a honeycomb pattern of the intensity distribution in reciprocal lattice space (continuous-line structure along the *fcc* zone boundary) providing the first direct evidence for nearly frustrated antiferromagnetism (AF) on the face centered cubic (*fcc*) lattice. A small but finite lattice distortion below 30.9 K lifts the degeneracy of the magnetic ground state due to the frustration and eventually result in the coexistence of the type I and the type II AF LROs, which are mutually incompatible in the *fcc* symmetry at higher temperatures.

75.25.+z, 75.40.Gb, 75.50.Ee

In spite of extensive theoretical and experimental explorations [1] of frustrated magnetism, search for such new examples is still very active. This class of materials does provide many new and unexpected phenomena including the high temperature superconductivity. Therefore the research and development for such materials constantly brings new challenges for theoretical interpretation. These materials often show the robust magnetic frustration phenomenon. A prototype is a Kagomé antiferromagnet, where the magnetic frustration is caused by solely rigid geometrical spin structure with a nearest neighbor (NN) antiferromagnetic (AF) interaction on a 2-dimensional (2D) triangular lattice [1]. Extensive studies of this model have revealed that suppression of a long range order (LRO) in geometrically frustrated compounds is directly affected by strong quantum fluctuations. Another example is the 3D antiferromagnet with corner-sharing tetrahedra such as transition metal pyrochlores and spinels [1]. On the other hand, one can introduce a fragile frustration phenomenon which is subject to both geometrical spin structure and a subtle balance among various magnetic interactions. Such a subtle balance is easily broken by structural phase transition (SPT) as observed experimentally [2,3].

In order to study the spin dynamics of these systems, the momentum and energy dependence of the generalized spin susceptibility $\chi''(\mathbf{q}, \omega)$ is indispensable. However in most cases, the lack of large enough single crystal prohibits the detailed studies on the momentum dependence, and often the parameters in the theoretical model have been set rather arbitrarily. It is emphasized here that the geometrical structure only is not enough to guarantee the frustration and degeneracy. In this paper we report the

neutron scattering experiment on the NiS₂ single crystal with *fcc* lattice structure. The detailed analysis of the scattering intensity provides the first direct evidence that the system is very near the phase boundary between the two types of antiferromagnetic long range order (AF LRO). This quasi-degeneracy is lifted by the SPT at low temperatures.

NiS₂ possesses anomalies in its thermodynamic properties [4–6] and an unusual coexistence of type I and type II antiferromagnetic (AF) LROs [7,8] which are incompatible from symmetry considerations for the undistorted *fcc* lattice. It shows magnetic phase transitions at low temperatures with persistent short range magnetic correlations up to high temperature in consequence of the frustrated magnetic structure of NiS₂ [6]. In addition, the structural instability pertinent to this compound was clearly observed both in dilatometric [9,10] and *X*-ray diffraction [11,12] measurements.

Extensive investigations for a series of transition metal dichalcogenides, MX₂, during the '70s [13] appeared to conclude that a simple view of the narrow band concept applied for the *d* electrons on M sites is sufficient to explain most of the experimental facts. However, the recent photoemission experiments indicate that NiS₂ is not even a simple Mott Hubbard insulator but rather a charge transfer insulator (CTI) [14]. Note that such CTIs are commonly realized in the strongly correlated electron systems of the progenitors of high *T_C* superconductor and colossal magneto-resistance materials.

Experimental study was done using 9 single crystals grown by the chemical vapor transport method, with a total volume of 0.9 cm³, which were aligned in the (*hkk*) reciprocal lattice zone using shiny (100) and (111)

facets. Neutron scattering measurements were performed on TOPAN spectrometer installed at the JRR-3M Reactor of the Japan Atomic Energy Research Institute. The crystal structure was determined to be of high symmetry (Pa3) above T_{N2} . Although a small distortion occurs below T_{N2} , it is ignored in our notation of the crystal symmetry presentation and we treat all the neutron scattering data within the fcc unit cell notation.

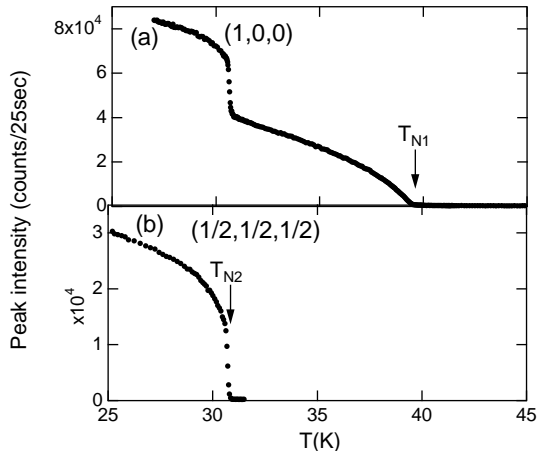


FIG. 1. The temperature dependence of the peak intensities of the type I (a) AF Bragg (100) and the type II (b) AF Bragg $(1/2, 1/2, 1/2)$ peaks.

Elastic neutron scattering measurements confirmed the existence of [7,12] two types of sharp Bragg reflections: the type I LRO with AF wave vector $\mathbf{Q}_I = (1, 0, 0)$ appears at $T_{N1} = 39.6\text{K}$ and the type II reflections with $\mathbf{Q}_{II} = (1/2, 1/2, 1/2)$ arise abruptly below $T_{N2} = 30.6\text{K}$ superposed on the type I AF LRO with rather discontinuous phase transition (Fig. 1). Furthermore, evaluation of the magnetic entropy estimated from the data of heat capacity reveals that the sum of the entropy released at *both* transitions (ΔS is 0.51 and 0.60 (J/mole-K) for T_{N1} and T_{N2} , respectively) is much smaller than $R \ln 3$ (9.13 J/mole-K). In order to probe spin fluctuations which is characteristic of these unusual properties of the phase transitions, we have performed inelastic neutron scattering measurements with momentum transfers in the $(h00) - (0kk)$ plane of reciprocal space where both the type I and the type II AF Bragg reflections are observable.

		temperature			
		0	(A) $T_{N2}=30.6\text{K}$	(B) $T_{N1}=39.6\text{K}$	(C) $T=150\text{K}$ $T=300\text{K}$
diffuse scattering	LRO and spin wave	type I + type II	type I	no Bragg reflection	
	$\mathbf{Q}-(1,0,0)$ (type I)	inelastic $\omega \sim 12\text{meV}$	inelastic $\omega \sim 12\text{meV}$	quasi-elastic scattering \dashrightarrow	
	$\mathbf{Q}-(\frac{1}{2}, \frac{1}{2}, \frac{1}{2})$ (type II)	inelastic $\omega \sim 12\text{meV}$	quasi-elastic scattering \dashrightarrow		
	zone boundary	none			

TABLE I. Three characteristic temperature regimes of magnetic excitations in NiS_2 .

Spin fluctuations in NiS_2 were found to be dramatically different in three temperature regions as shown in Table 1. (A) In the first regime of the paramagnetic phase above T_{N1} , strong antiferromagnetic spin correlations persist up to high temperatures. Spin fluctuations in this phase are manifested by two components: (i) magnetic diffuse scattering around the type I AF Bragg point and (ii) magnetic diffuse scattering component along the fcc zone-boundary around the type II AF Bragg point. Both components are observable even at room temperature but grow below 150K, where anomalies in the conductivity appear. (B) In the second, intermediate regime $T_{N2} < T < T_{N1}$, type I AF LRO arises and concomitantly spin-wave excitations occur. Two diffusive magnetic scattering components still exist as well. However, the diffuse scattering around the type I AF Bragg point becomes rather inelastic as described below. (C) In the low temperature regime below T_{N2} , where both the type I and II AF LROs are present with a possible rhombohedral lattice distortion, the spin waves for each AF LRO were observed. On the other hand, the diffuse scattering around both the type I and II AF Bragg points becomes inelastic and the zone boundary component disappears [15].

Next, we present the detailed experimental results for the intermediate regime B followed by theoretical analysis. At $T = 32\text{K}$, we measured the \mathbf{Q} -scans for the fixed energy transfers of $\omega = 2\text{meV}$ and 10meV along the [100] direction around the $(0, 1 + \zeta, 1 + \zeta)$ points with $\zeta = 0, 0.125, 0.25, 0.375, 0.5$ (Fig. 2a). For energy transfer $\omega = 2\text{meV}$ (open circles), a well defined single peak was observed for $0 \leq \zeta \leq 0.25$, whereas it splits into two distinct peaks for $0.25 < \zeta \leq 0.5$. Note that the peak for $\zeta = 0$ coincides with the type I AF Bragg point $(0, 1, 1)$ and that both $(\pm 1/2, 3/2, 3/2)$ peaks are at the type II AF Bragg points. These peaks are located on the zone-boundary line of the fcc lattice as shown by broken line forming a honeycomb pattern in Fig. 2a. The same set of scans with $\omega = 10\text{meV}$ (closed circle) reveal basically the same geometric picture, although the signal intensity is more concentrated around the type I AF Bragg point. (We define this as a type I peak.) The neutron scattering signal is purely magnetic, since the scattering intensities at momentum transfer (300) follows the square of the Ni^{2+} ion magnetic form factor.

We observed that the type I peak persists even at $\omega = 16\text{meV}$ with a frequency-independent peak width of 0.11\AA^{-1} . Based on this observation, we conclude that this mode is intrinsically inelastic at the intermediate temperature regime (B). This conclusion is supported by the energy-scans with fixed \mathbf{Q} at the type I AF Bragg point (011) in Fig. 2b. Furthermore, \mathbf{Q} -scans at the type I point along [100] and [011] directions show that the *magnetic scattering with $\omega > 10\text{meV}$ around the type I Bragg point exhibits an isotropic peak in the $(h00)-(0kk)$ plane.* We then observed a lower energy diffuse com-

ponent around the type II AF Bragg point, which has a much stronger intensity than the type I peak. The \mathbf{q} width and scattering intensity of this component does not change with \mathbf{q} along the line connecting the (0,1.25,1.25) and (0.5,1.5,1.5) points within the limit of experimental errors. Therefore, we conclude that *the magnetic scattering around the type II Bragg point is extended on the fcc zone boundary*. This component was concluded to be quasi-elastic by confirming energy scan at (1, -0.3, -0.3) which is close to the zone-boundary line.

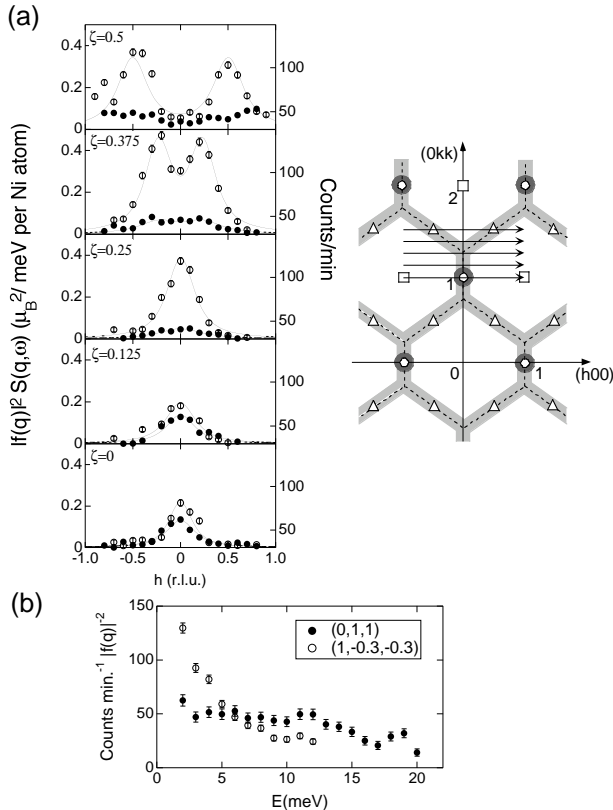


FIG. 2. (a) Constant-energy scans along the [100] direction at 32 K. Open and closed circles represent the data for $\hbar\omega = 2$ and 10 meV, respectively. The horizontal collimator is B-30'-60'-B with $E_f = 14.7$ meV. Absolute units for $S(\mathbf{q}, \omega)$ were calibrated using the intensity of the transverse acoustic phonon. The right panel shows Reciprocal space for the fcc lattice. The broken line shows the honeycomb zone boundary of the fcc lattice in the (h00)-(0kk) plane. Open circles, triangles and gray rectangles represent the AF type I, type II, and nuclear Bragg points, respectively.

(b) Constant- \mathbf{Q} scans at the type I AF Bragg point (011) and near the fcc zone boundary (1,-0.3,-0.3) at 32 K. Open and closed circles show the data at (011) and (1,-0.3,-0.3), respectively. The data are divided by the square of the magnetic form factor at each position after subtraction of the background.

To extract information from the observed geometrical pattern of the critical scattering, we studied the momentum-transfer dependence of the energy integrated

scattering law $S(\mathbf{Q}) = \int d\omega S(\mathbf{Q}, \omega) / |F(\mathbf{Q})|^2$ ($F(\mathbf{Q})$ is the magnetic form factor), which is proportional to the real part of the static momentum dependent magnetic susceptibility. Both above and below the Néel temperature T_{N1} the static susceptibility can be expressed in following form, $\chi'(\mathbf{Q}) \sim \{\delta + (1 - \mathcal{L}(\mathbf{Q})/\mathcal{L}(\mathbf{Q}_{AF}))\}^{-1}$. The parameter δ specifies how much the actual temperature deviates from T_{N1} , \mathbf{Q}_{AF} is an AF wave vector where the divergence of susceptibility at $T = T_{N1}$ occurs, and $\mathcal{L}(\mathbf{Q})$ represents the Fourier transform of the interaction matrix. Considering the NN J_1 , next NN J_2 and next next (third) NN J_3 AF interactions, one can express the Fourier transform of the interaction matrix $\mathcal{L}(\mathbf{Q}) = -|J_1| \{\phi_1(\mathbf{Q}) + R_2\phi_2(\mathbf{Q}) + R_3\phi_3(\mathbf{Q})\}$ in terms of the standard fcc lattice geometrical factors ϕ_i and ratios $R_2 = J_2/J_1$ and $R_3 = J_3/J_1$.

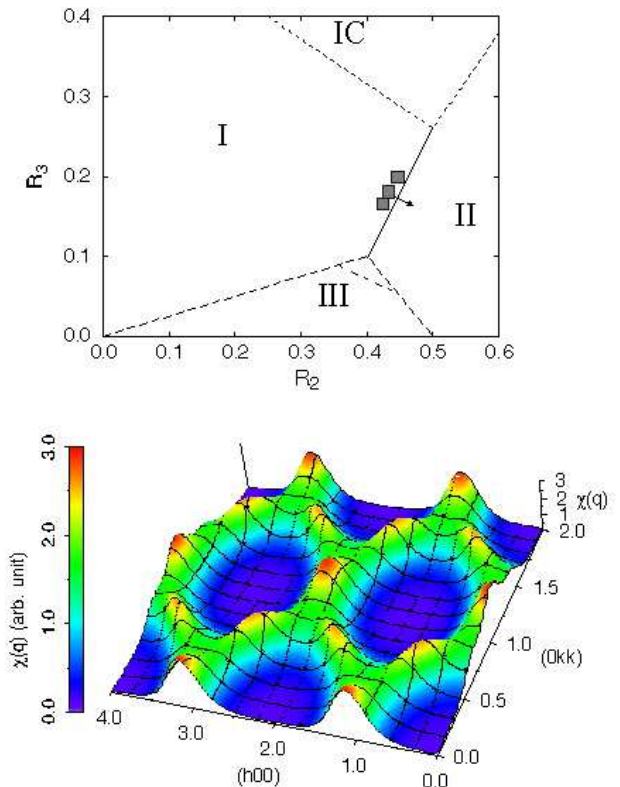


FIG. 3. Upper panel: Magnetic phase diagram of the fcc lattice. Type I, type II and type III ($\mathbf{Q}_{AF} = (1, 1/2, 0)$) phases are indicated by I, II, and III, respectively. The area denoted by IC and the small triangle near the crossing of the lines separating I-II and II-III phases are regions where incommensurate phases are found. Gray rectangles are possible locations of NiS_2 in the phase diagram in the high symmetry phase. The arrow represents the possible change of the position in the diagram due to rhombohedral structural distortion.

Lower panel: Surface of critical scattering intensity for $R_2 = 0.434$, $R_3 = 0.164$, and $\delta = 0.3$.

Since the value of the AF wave vector depends only on the parameters R_2 and R_3 , we analyzed the phase dia-

gram in terms of these coordinates (Fig. 3, upper panel). We found that the honeycomb structure (Fig. 3, lower panel) of the critical scattering in the $(h00) - (0kk)$ plane is a general feature of the *fcc* lattice with the AF interactions up to third NN. This pattern is robust in a rather large domain where $R_2 < 0.6$ and $R_3 < 0.3$. Therefore, to locate the position of NiS₂ in the phase diagram, one have to study the fine features of the honeycomb structure that are general for the *fcc* lattice. To fix the values R_2 and R_3 for NiS₂ in the high-symmetry phase, i.e. for $T > T_{N2}$, we calculated the critical scattering pattern at numerous points in phase I, and found three points (gray rectangles in upper panel of Fig. 3) that obey the following conditions obtained experimentally: (i) the scattering around the type I AF Bragg point is a symmetric circle-like peak; (ii) the contour plot of the scattering intensities around the type II AF Bragg points are ellipses aligned along the *fcc* zone boundary; and (iii) energy integrated intensities at the type I and the type II AF Bragg points are equal within the limit of experimental errors. Therefore, one can conclude that NiS₂ in a high-symmetry phase is situated in the vicinity of the gray rectangles and, hence, very close to the border separating the I and II phases (see Fig. 3) [16]. This quasidegeneracy also explains the anomalous temperature dependence of the spin fluctuations above T_{N1} (regime A), namely the type I AF LRO temperature is suppressed by the frustrated magnetism, and the magnetic diffuse scattering is expected for a wide temperature range above T_{N1} .

Here, we discuss the fact that the two components of magnetic scattering have different properties in the intermediate temperature regime (B). These components belong to different irreducible representations of the symmetry group of the cubic lattice.

Even when the type I AF LRO is established, both components are still present. Hence, the virtual ground state of the type II caused by magnetic frustration is quasidegenerate with the actual type I magnetic ground state of the cubic lattice. We emphasize that the quasidegeneracy occurs only accidentally between the two ground states which is incompatible in the cubic lattice symmetry (i.e. can be removed by a change of AF couplings) according to the Wigner theorem in group theory. Therefore, the system is not exactly frustrated but nearly frustrated. However, the nearly frustrated situation can be resolved by the structural distortion which lowers the lattice symmetry. As a consequence, the type I and the type II AF LROs become compatible in the reduced symmetry group. In order to elucidate possible consequences of SPT we studied small deviations of the magnetic exchange parameters constrained by the symmetry of the rhombohedral phase. Then we found that comparatively small changes of magnetic couplings ($< 10^{-2}$) can induce a shift in the phase diagram denoted by the arrow in Fig. 4. A notable feature of the lowest

transition at T_{N2} is that the *system avoids the phase of nearly frustrated magnetic interactions by lowering the lattice symmetry*.

In conclusion, in the paramagnetic and high symmetry phase (A) above T_{N1} , NiS₂ is a paramagnet where anomalies are governed by geometrical frustration and competing interactions. The second-order transition at T_{N1} into the LRO type I AF state does not remove the nearly frustrated situation. The magnetic diffuse scattering along the *fcc* zone boundary, indicating the quasidegeneracy of the type I and II AF LROs, persists down to the frustration-avoiding SPT at T_{N2} , where the type I and the type II phases probably become compatible due to the rhombohedral structural distortion.

Authors are indebted to S. Maekawa, W. Koshibae and D. Belanger for stimulated discussions. M. Matsuura has been supported by Research Fellowships of the Japan Society for the Promotion of Science for Young Scientists.

-
- [1] For a review see A. P. Ramirez, in “Magnetic Materials” (North-Holland, Amsterdam, to be published).
 - [2] S.-H. Lee *et al.*, Phys. Rev. Lett. **84**, 3718 (2000).
 - [3] R. Melzi *et al.*, Phys. Rev. Lett. **85**, 1318 (2000).
 - [4] X. Yao *et al.*, Phys. Rev. B **54**, 17469 (1996).
 - [5] X. Yao *et al.*, Phys. Rev. B **56**, 7129 (1997).
 - [6] M. Matsuura *et al.*, J. Phys. Soc. Japan **69**, 1503 (2000).
 - [7] J. M. Hasting, L. M. Corliss, IBM J. Res. Dev. **14**, 227 (1970).
 - [8] K. Kikuchi *et al.*, J. Phys. Soc. Japan **45**, 444 (1978).
 - [9] H. Nagata, H. Ito, T. Miyadai, J. Phys. Soc. Japan **41**, 2133 (1976).
 - [10] T. Miyadai, M. Saitoh, Y. Tazuke, J. Magn. Magn. Mat. **104-107**, 1953 (1992).
 - [11] H. S. Jarrett *et al.*, Mat. Res. Bull. **8**, 877 (1973).
 - [12] T. Thio, J. W. Bennett, T. R. Thurston, Phys. Rev. B **52**, 3555 (1995).
 - [13] J. A. Wilson, *The metallic and non-metallic states of matter* (Taylor & Francis, 1985) Chap. 9.
 - [14] A. Fujimori *et al.*, Phys. Rev. B **54**, 16329 (1996).
 - [15] T. Thurston *et al.*, unpublished data.
 - [16] The LDA + U calculation gives values of J_1 , J_2 , J_3 which are consistent with this estimation in upper panel of Fig. 3; I. V. Solovyev, A. Mishchenko, N. Nagaosa, in preparation.